Title page

Behavioral phenotypes of SCN-specific *Dicer* knockout mice

Ngoc-Hien Du[1]*, Konstantinos Kompotis[1], Miho Sato[1], and Steven Brown[1]

[1]Institute of Pharmacology and Toxicology, University of Zurich, 8057 Zurich, Switzerland

*Correspondance: Ngoc-Hien Du, hiendngoc@gmail.com, ORCID iD: 0009-0007-3525-8094.

Present address: Ngoc-Hien Du, Laboratory for Biomedical Microfluidics, Swiss Federal Institute of Technology Lausanne (EPFL), Rue du Bugnon 25A, 1005 Lausanne, Switzerland.

Keywords: SCN-specific *Dicer* knockout, miRNAs, locomotor activity, period length, circadian rhythms

Acknowledgements: NH. D. designed and performed the study. K. K. performed the injections for the inducible knockout model. M. S. performed the immunostaining experiments. NH. D. carried out the analysis. NH. D., K. K., and M. S. wrote the manuscript. We thank Sara Pierre for helping with the MEA recording. We thank Professor David Gatfield for providing the *Dicer*^{flox} mice as well as infrastructure to carry out part of the wheel running experiments. We thank Professor Steven Brown for the supervision of the project and mentorship.

Conflict of interest disclosure: The authors declare no conflict of interest.

Abstract

The suprachiasmatic nucleus (SCN) is the master clock that orchestrates circadian clocks across the body to synchronize with and anticipate the earth's light/dark cycles. Although post-transcriptional regulators called microRNAs have been implicated in physiological SCN function, how the absence of the entire mature miRNome impacts SCN output has not yet been explored. Here, we have generated an SCN-specific *Dicer* knockout mouse model by crossing *Syt10*^{Cre} mice with *Dicer*^{flox} mice to study behavioral consequences of miRNA depletion in the SCN. We show that loss of all mature miRNAs in the SCN shortens the circadian period length by ~40 minutes at the tissue level, and by ~50 minutes at the locomotor activity level. Knockout animals also showed arrythmicity or ultradian locomotor activities with no light masking under constant light, a condition which usually caused lengthening of the circadian period length and reduced activities, i.e. light masking, in nocturnal animals. Moreover, induction of *Dicer* knockout by Cre injection into the SCN of adult *Dicer*^{flox} mice eventually resulted in loss of behavioral rhythms. Finally, we show suggestive evidence that SCN desynchronization might be one mechanism underlying the behavioral phenotypes of SCN-specific *Dicer* knockout animals.

Introduction

Circadian rhythmicity relies on a hierarchical system of clocks coordinated by a master clock residing in the brain region called the suprachiasmatic nucleus (SCN)[1]. This small nucleus lies just above the optic chiasm, and receives direct photic information from the ganglion cells of the retina[2]. The master clock then orchestrates peripheral clocks throughout the organism to synchronize with the environment[3,4]. At the organismal levels, the circadian clocks exert their function on vital behaviors such as sleep/wake cycles, and feeding/fasting rhythms[4]. At the molecular level, the output of all autonomous clocks is rhythmic gene expression with a period of about 24 hours[5]. Interestingly, a large proportion of the transcriptome, ~43% in mouse[6], 44% in human[7], and 82% in primate[8], is rhythmically expressed somewhere in the body.

Circadian gene expression originates not only from circadian transcription, but also from circadian post-transcriptional and post-translational mechanisms[9,10]. A recent meta-analysis and modeling approach estimated that 30% of circadian transcripts are regulated post-transcriptionally in mouse liver[11]. Among the known post-transcriptional mechanisms, the short (19-25 nucleotides) non-coding RNA molecules coined microRNAs (miRNAs) play a crucial role in shaping the dynamics of gene expression, by regulating both mRNA degradation and translation of a multitude of target genes. There are more than 1000 miRNA genes in the human genome that target up to 60% or protein coding genes[12,13], with one miRNA targeting from a dozen to hundreds of mRNA targets[14]. In the last two decades, miRNAs have emerged as important players in regulating all kinds of biological processes, including circadian rhythms, from the molecular to the behavioral level.

The involvement of miRNAs in circadian oscillations has been reported in cell lines[15], in peripheral tissues[16], as well as in the SCN[17,18]. However, most studies focus on the role of an individual miRNA in a specific context. Informative as it may be, this approach often cannot showcase the magnitude of miRNA influence on a biological system. We previously demonstrated a comprehensive view of miRNA regulation of the hepatic transcriptome employing a genetic mouse model in which miRNA biosynthesis was inactivated (liver-specific *Dicer* knockout)[19]. In our hands, miRNAs played an essential role in adjusting the phase and amplitude of 30% of the circadian transcriptome in mouse liver.

To study the roles of miRNA ensemble in shaping the function of the master clock, we have now extended the use of tissue-specific *Dicer* knockout model from the liver to the SCN. We report here that the SCN-specific *Dicer* knockout variably altered both tissue and behavioral circadian period length in two different mouse models. We also provide suggestive evidence that should be taken into consideration in future investigations of the molecular mechanisms underlying the behavioral phenotypes.

Materials and Methods

Animals

All animal experiments were performed according to the cantonal guidelines of either the Canton of Vaud, Switzerland, license 2376.1, or the Canton of Zurich, Switzerland, license 060/2017. Animals were allowed to access food and water *ad libitum* under a 12:12-hr light dark (LD) cycle, unless otherwise stated. *Dicer^{flox}* mice (IMSR_JAX:006366) were gift from Professor David Gatfield[19], *Syt10^{Cre}* knock-in mice (MGI:5286607) were gift from Dr. Henrik Oster[20], *Period2::Luciferase* (*Per2::Luc*) knock-in mice (MGI:3040876) were gift from Dr. Joseph Takahashi[21]. Genotype of the animals were examined by PCR as described in the original publication of each mouse strain. Due to the expression of *Syt10* in the testis, males homozygous for *Syt10^{Cre}* should not be used for mating. Male of genotype *Dicer flox/flox; Syt10^{Cre}* +/+ were crossed with female *Dicer flox/flox; Syt10^{Cre}* KI/+ to create knockout of genotype *Dicer flox/flox; Syt10^{Cre}* KI/+ and control of genotype *Dicer flox/flox; Syt10^{Cre}* +/+. Animals aged between 2-6 months were used for the experiments. Litter mates or animals of similar ages were used for the same experimental conditions.

Genotyping

Polymerase chain reaction (PCR) was used for genomic DNA extracted from either the tail, ear or olfactory bulb to genotype each tissue or animal. To genotype alleles of *Dicer*, the following two primers were used: DicerR1, AAACATGACTCTTCAACTCAAACTCAAACG, and DicerF1, AATATTAATCCTGACAGTGACGGTCCAAAG. To confirm deletion of exon 23, primer DicerF1 and DicerDel, GGGCAGCCCCATCTCAAAGGCCTACCTGAG were

used. To genotype alleles of *Syt10*, the following three primers were used: Syt10 F, AGACCTGGCAGCAGCGTCCGTTGG; Syt10 R, AAGATAAGCTCCAGCCAGGAAGTC; Syt10 KI, GGCGAGGCAGGCCAGATCTCCTGTG. To genotype alleles of *Per2::Luc*, the following three primers were used: P1, CTGTGTTTACTGCGAGAGT; P2, GGGTCCATGTGATTAGAAAC; P3, TAAAACCGGGAGGTAGATGAGA.

Tissue explants and bioluminescence recording and analysis

Dicer^{flox}; *Syt10*^{Cre} mice were crossed to *Per2::Luc* mice for bioluminescence recording of tissue explants. To prepare tissue explants, animals were sacrificed, and each tissue was collected into ice-cold HBSS (Cat# 14025, Life Technologies, CA) with 10 mM Hepes (Cat# H0887, Sigma, MO). For SCN and pituitary, brains were sliced at 300 μm interval with a McILWAIN Tissue Chopper, and each area was isolated separately in ice-cold HBSS buffer with Hepes. For kidney, liver, tail and lung, pieces of tissues were sliced at 300 μm interval. Each tissue explant was cultured on either millicell (#PICMORG, Merckmillipore, MA) or a piece of hydrophilic PTFE-membrane (#BGCM00010, Merckmillipore, MA) submerged with DMEM (Cat# D2902, Sigma, MO) with 0.035 % Sodium bicarbonate (Cat# S8761, Sigma, MO), 10 mM Hepes (Cat# H0887, Sigma, MO), 4.5 g/L D-glucose (Cat# G8769, Sigma, MO), 1.0 % Penicillin-Streptomycin (Cat# 15070-063 , Life Technologies, CA), 2% B27 (Cat# 17504044, Gibco) and 0.1 mM D-Luciferin (Promega, WI). Circadian bioluminescence was recorded with photomultiplier tubes (PMTs) every 48 mins at 34.5 °C with 5% CO_2. To assess period length of the bioluminescence *ex vivo*, the original data were subtracted with 24-hr running average and sinusoidal curve fitting was applied using Lumicycle analysis software (Actimetrics).

Locomotor activity recordings and analysis

Mice were individually housed in cages containing running wheels, or with infrared detectors as indicated, with *ad libitum* access to food and water. Data was collected and analyzed using ClockLab software (Actimetrics). For jetlag experiment, onset was extracted using ClockLab software, and the phase shift half time, defined as the time at which half the phase shift was completed was extracted using drda R package[22].

Immunohistochemistry

Animals were deeply anaesthetized with Pentobarbital and intracardially perfused with 10 ml of ice-cold saline, followed by 20 ml of ice-cold 4% paraformaldehyde / 0.1 M phosphate buffer (PB, pH 7.4). Brains were collected and post fixed in 4% paraformaldehyde with 0.1 M PB for overnight at 4 °C followed by cryoprotection in 20% sucrose / 0.1 M PB for 48 hrs at 4 °C. The brains were sectioned by 30 μm with cryostat at -17 °C and washed in 0.1 M PB at room temperature. The sections were treated with 5% goat serum, incubated either with or without 1:1000 primary antibody

(α-Vip (Cat# T-4246, Peninsula laboratories, RRID: AB_518682) with 2% NGS in PBS with 0.05% Triton (PBS-Triton), rinsed in PBS and PBS-Triton, incubated with 1:1000 secondary antibody (Goat α-Rabbit IgG labelled with Cy3, Cat# ab6939, abcam, RRID: AB_955021) with 2% NGS in PBS-Triton, and then rinsed in PBS and PBS-Triton. The sections were mounted onto gelatin-coated microscope slides, air-dried, and dehydrated with Fluoromount™ Aqueous Mounting Medium (Cat# S3023, Dako). Fluorescent images were obtained with a widefield microscope Apotome (Zeiss, Germany).

Multi-electrode recordings and analysis

Mice were sacrificed and brains were quickly removed at ZT2 (ZT0 is light on time, ZT12 is light off time). Brains were sliced coronally with the vibratome (#7000smz-2, Campden Instruments) by 300 µm in ice cold artificial cerebro-spinal fluid (ACSF, in mM: NaCl 95; KCl 1.8; KH_2PO_4 1.2; $CaCl_2$ 0.5; $MgSO_4$ 7; $NaHCO_3$ 26; glucose 15; sucrose 50; oxygenated with 95% O_2; 5% CO_2; pH 7.4, measured osmolarity 310 mosmol kg-1). After 30 minutes incubation, a 300µm slice containing the SCN was placed on a 60pMEA100/30iR-Ti-gr perforated array (Multi Channel Systems). Slices were positioned so that the entire SCN was in contact with the electrode region of the array, and kept in place with a weight, with suction from underneath to maximize contact between the slice and the electrodes. Oxygenated ACSF at 34°C ran continuously through the MEA chamber for the duration of the experiment (1.2ml/min inflow / 17ml/min outflow + gravity flow inflow/suction outflow at 65). Field potential was detected by the MEA at 20,000 Hz using *Multi-Channel Experimenter* (Multi Channel Systems). Data was recorded every 30 minutes. Because of the large file size, recordings were limited to 10 minutes at the beginning of each 30 minutes for the duration of the experiment. Data were analyzed using Offline Sorter (Plexon) as follows: files were run through a butterworth high pass filter at 300 Hz and 'spikes' were detected using a threshold of ± 4 Standard Deviations. For each spike the waveform was analyzed and a unit assigned to each unique waveform detected from an individual electrode using the Valley Seeking spike sorting algorithm. Spikes were distinguished from noise by waveform. Data were analyzed using NeuroExplorer v5. Only spikes with mean frequency > 0.5 Hz were used.

Injection of AAV constructs expressing *hSyn-Cre* in the SCN

Male *Dicer^{flox}* mice (12-16 weeks old) were stereotactically (Kopf Instruments, CA, USA) injected under isofluorane anesthesia, bilaterally at the SCN (ML= ± 0.18 mm; AP= 0.46 mm; DV= 5.8 mm; relative to bregma). The following viruses were injected at a volume of 300 nl with a rate of 150 nl/min: For knockouts (n=6), ssAAV9/2-hSyn1-chl-mCherry_2A_iCre-WPRE-SV40p(A) (UZH Vector Core, $7.9x10^{12}$ viral particles/ml; iCre: Addgene #24593) and for controls (n=7), ssAAV9/2-hSyn1-chl-mCherry-WPRE-SV40p(A) (UZH Vector Core, $4.8x10^{12}$ viral particles/ml). Post-surgery, mice were returned to the housing cage, and allowed to recover. After the passage of three weeks to ensure recombination and adequate expression of the AAV constructs, locomotor activity (using running wheel) was recorded under various light-dark conditions. Following the completion of the experiment, mice were

perfused with 4% paraformaldehyde (PFA), their brains extracted, and sites of injection were confirmed through mCherry expression with confocal microscopy. Mistargeted animals were excluded from further analyses.

Results

Generation of SCN-specific miRNA depletion mouse model

To study the function of miRNAs in the SCN, we generated a mouse model in which miRNA biogenesis is inactivated in the majority of the SCN cells. We bred mice carrying conditional knockout alleles for the *Dicer1* gene (referred to as $Dicer^{flox}$ in the following), and mice carrying *Cre* recombinase cDNA inserted into the *Synaptotagmin 10* locus (referred to as $Syt10^{Cre}$), a gene strongly expressed in the SCN[20], and obtained $Dicer^{flox}$; $Syt10^{Cre}$ mice, called here SCN-specific *Dicer* knockout (KO) mice. Due to the small size of the SCN and potential contamination from surrounding tissues that limits its use in PCR analysis, the olfactory bulb, which also expresses *Syt10*, was used for PCR analysis to confirm successful recombination at the $Dicer^{flox}$ locus (Figure S1). PCR analysis of the ear showed no detection of the recombined allele as expected.

SCN-specific Dicer knockout showed shorter free-running period with variable onsets

We found that knockout animals had shorter free-running period than control animals (Figure 1, knockout mean = 22.93 h, control mean = 23.78 h, $t_{Welch}(9.23) = 5.33$, p = 4.35e-04). Knockout animals also reentrained almost immediately to a new light-dark cycle after 6 h phase advance (Figure 2A, C). Analysis of the phase shift half time, i.e. time required to reach half of the phase shift, showed that knockout animals required only 0.63 ± 0.60 days while controls required 2.37 ± 0.25 days to reach 3h phase shift. There was a tendency of faster re-entrainment to 6 h phase delay in knockout animals vs controls (Figure 2B, D). The delay phase shift half time was 0.31 ± 0.57 days and 0.76 ± 0.08 days for knockouts and controls, respectively. The high variation for knockouts in the phase delay experiments was due to low mouse number. It is noticeable that the standard deviation of phase shift half time was higher in knockout than that in controls, due to apparently variable activity onsets, for which we quantified further below.

We found that knockouts showed activity onsets that were different to light-off time by 31.9 ± 12.1 minutes, while controls showed only 7.3 ± 5.2 minutes activity onset differences (Figure 3A, ttest p = 8.2e-05). For the knockout animals, the differences were mostly due to earlier wake-up while there were also occasions where the animals showed activity onset after the light-off time. In addition to the less precise activity onset time, knockout animals showed larger variation in their activity onsets compared to control animals. Under LD = 12:12, the standard deviation of onset time was 44.1 ± 20.3 minutes for knockouts and 6.1 ± 3.1 minutes for controls (Figure 3B, ttest p = 4.4e-05). Since running wheel might change the animals' behaviors, we measured onset in another cohort of animals using infrared detector

(Figure 3C, Figure S2). In spite of the difference in the devices, we found again that knockout animals showed larger standard deviation of 43.6 ± 7.0 minutes in their activity onsets, compared to 16.0 ± 8.4 minutes for controls (Figure 3C, ttest p = 1.4e-04). The large standard deviation in activity onsets of knockouts was consistent with all tested 24-hour period light-dark conditions with different day length (Figure 4). Reasoning that shorter period length of knockout animals might enable easier entrainment to shorter environmental cycles, we measured activity onset under LD = 11:11. Indeed, knockout animals showed smaller onset variation than controls (Figure 3D, knockout = 0.97 ± 0.34 h, control = 2.35 ± 1.12 h, ttest p = 0.038). These results suggest that, due to the shorter internal period length, it was more challenging for knockout animals to get entrained to the light/dark cycles of 24 hours. However, we cannot rule out that larger onset variation is due to defects in SCN synchrony. Therefore, we next investigated knockout behaviors under conditions that challenge SCN synchrony.

Lack of miRNAs in the SCN caused arrhythmicity and lack of light masking under constant light condition

Since constant light condition (LL) has long been used to disrupt circadian rhythms[23], mice lacking Dicer in their SCN were recorded under LL condition (Figure 5). We observed that control animals under LL exhibited longer period length for the duration tested (Figure 5B), whereas knockout animals showed arrhythmicity or ultradian rhythms (Figure 5A). Unlike control animals, knockout animals did not show light masking, i.e. reduced activities under constant light condition observed in nocturnal animals. Increasing light intensity during the LL condition did not affect the lack of the masking effect in knockout animals (data not shown). Interestingly, knockout animals did show masking response at the beginning of the LD = 3:3 condition (Figure 6), an ultradian light condition that has been shown to disrupt circadian rhythmicity[24]. This suggests that knockout animals did not show light masking response under constant light condition, despite remaining responsive to light.

SCN tissue explants from SCN-specific Dicer knockout also showed shorter period length

To confirm if the short circadian period in the behavior of knockout animals was due to the disrupted SCN, we bred *Dicer^{flox}*; *Syt10^{Cre}* mice with *Period2::Luciferase (Per2::Luc)* knock-in mice and cultured their tissue explants from different tissues (Figure 7). Knockout tissue indeed showed shorter period length in an SCN-dependent manner (Figure 7A, knockout SCN mean = 24.21 h, control SCN mean = 24.83 h). We also observed that pituitary from knockout animals showed shorter period length (knockout pituitary mean = 23.76 h, control pituitary mean = 24.74 h), as expected from the expression of *Syt10* in the pituitary[25]. It is worth noting that during SCN explant preparation, SCN from knockout animals detached more easily

from the optic chiasm, and the amplitude of PER2::LUC oscillations in the SCN knockouts often damped faster than control slides (Figure 7B).

Inducible SCN-specific Dicer knockout showed shorter period length that eventually led to arrhythmicity

To rule out the effect of extra-SCN expression of *Syt10*, as well as the effect of possible developmental process, on the period length phenotype observed in our knockout model, we induced *Dicer* knockout in the SCN by injecting AAV expressing *hSyn-Cre* to the SCN. Two weeks after injection, behavioral phenotypes were assessed by recording wheel running activities (Figure 8). We found that induced knockout animals exhibited either directly arrhythmicity or a shorter period length that eventually led to arrhythmicity under any of the light conditions tested.

Indication that desynchronization might be one mechanism explaining the behavioral phenotype of Dicer knockout animals

We next sought the possible mechanisms underlying the behavioral phenotypes observed in knockout animals. It has been previously demonstrated that the vasoactive intestinal peptide (VIP), expressed in the SCN by a neuronal population receiving first the photic stimulus from the retinal ganglion cells, is the main synchronizer of the SCN neuronal networks[26]. Therefore, investigating the expression of VIP in the SCN of genetically *Dicer* knockout animals was the first reasonable step. We found suggestive evidence that VIP expression was reduced in the SCN upon depletion of miRNAs (Figure S3). Subsequently, we measured SCN network synchronization by recording neuronal activity of brain slices on multi electrode array (MEA). We found that only a portion of SCN from knockout retained its firing ability, conversely to slices from control animals in which the whole SCN fired in synchrony (Figure 9). Although these observations need to be recapitulated in a larger number of animals, taken together they suggest that SCN desynchronization may be one of the mechanisms underlying the behavioral phenotypes observed in knockout animals.

Gender differences observed in Dicer knockout animals

We observed that knockout females reached extreme weight (Figure S4A at 13-month-old, knockout females weighed 59.9 g, while control females weighed 32.7 g, both n = 2). Knockout females were also less fertile. Over a period of one year, from 10 breeding pairs between control males and knockout females, one pair produced 4 litters, four pairs produced 2 litters, and five pairs produced only one litter before pausing pregnancy. Regarding the circadian period, SCN tissue explants from KO females showed shorter period compared to controls as in males (Figure S4B, knockout SCN mean = 24.50 h, control SCN mean = 25.36 h). Surprisingly, we found that tissue explants from pituitary gland of control females showed shorter period compared to their SCN counterparts (control pituitary mean = 23.07 h), while

the two tissues from control males showed similar period (male pituitary mean = 24.74 h, male SCN mean = 24.83 h). In contrast, in knockout females, tissue explants from pituitary gland exhibited similar period length (knockout female pituitary mean = 24.33 h) compared to their SCN counterparts, as in males.

Discussion

In the current study, we explored the circadian consequences of depleting miRNAs in the master clock of the mouse brain. We report here a shorter period length in genetic knockout animals; and an initially variable, but finally arrhythmic, circadian behavior in inducible adult knockouts. One variable aspect between the two knockout models that might account for the difference in the observed phenotypes is the potentially incomplete deletion of *Dicer* in the SCN of the genetic knockouts. Indeed, it was previously shown that when using a *Syt10^{Cre}* mouse model to obtain SCN-specific *Bmal1* knockouts, BMAL1 expression was deleted in the SCN in a Cre dose-dependent manner[20]. However, due to the expression of *Syt10* in the testis and that whole body *Dicer* knockout is embryonic lethal[27,28], it is not possible to obtain tissue specific *Dicer* knockout mice that are homozygous for *Syt10^{Cre}*. We suggest that the incomplete deletion *of Dicer* in the SCN can be confirmed by performing *in situ* hybridization of *Dicer* in the SCN. Complete *Dicer* deletion might then lead to cell apoptosis in the SCN as has been seen in excitatory forebrain neuron-specific *Dicer* knockout model[29]. Since SCN lesion animals are arrhythmic, we cannot exclude that SCN cell death could explain the arrhythmic phenotype in the inducible knockout model. Another possible mechanism explaining the difference between genetic and induced knockouts is compensation by neuronal plasticity during development. This can be confirmed, for example, by knocking out *Dicer* in neonatal SCN slices by infection with AAV expressing *hSyn-Cre*.

Surprisingly, the genetic *Dicer* knockout also exhibited a female specific phenotype, namely obesity and compromised fertility. As reported in the original paper[20] and elsewhere, *Syt10* is highly expressed in the SCN, although it can be found also in the olfactory bulb and in the pituitary[20,25] . Therefore, we cannot rule out that the expression of *Syt10* outside of the SCN contributed to the above female *Dicer* knockout phenotypes. Furthermore, we found that wild-type female mice's tissue explants from pituitary showed shorter period length compared to the SCN tissue explants from the same animals, a phenotype that was not observed in wild-type males. In fact, gender differences in circadian phenotypes has been described previously. For example, females re-entrain to new light-dark cycle rapidly at proestrus than at metestrus[30]. The fast re-entrainment of locomotor activity is accompanied with fast clock phase shifts in peripheral tissues but not the SCN. The observed phenotypes could be conveyed also via pro-opiomelanocortin (POMC) neurons, which receive direct input from the SCN, and have been previously implicated both in hyperphagia and obesity[31], as well as sexually dimorphic functions in the context of energy homeostasis[32]. Future studies should explore the relationship between SCN and extra-SCN regions when using *Syt10^{Cre}* mouse model, in both males and females.

Dicer knockout animals exhibited faster entrainment to a new light/dark cycle, which is a phenotype observed also in mice lacking two vasopressin receptors V1a and V1b[33] or LIM homeobox transcription factor Lhx1[34]. In both vasopressin receptors and Lhx1 deficient model, reduced interneuron coupling is the molecular mechanism underlying the lack of resistance to a new light/dark cycle. These are aligned to our suggestive evidence that SCN desynchronization is the cause for the behavioral phenotypes. However, experiments with more animals need to be done to confirm the reduced VIP expression as well as reduced firing rate in the SCN of knockout animals. In the cortex, VIP is a predicted target of miR-28-3p[35]. While miR-28-3p is expressed in olfactory bulb, hippocampus, striatum, and the spinal cord, it is not expressed in the cortex, where VIP is highly expressed. The reduction of VIP expression in the *Dicer* knockout SCN therefore, could be an indirect consequence of miRNA depletion. Further investigation of the underlying mechanism(s) should examine the role of neuropeptide communication in the observed phenotypes. For example, grafting control SCN onto knockout SCN might be able to rescue the period length phenotypes.

Finally, determining the responsible miRNA(s) is crucial to understand miRNA-dependent regulation of the SCN network. Recently, whole body deficiency in miR-183/96/182 cluster was shown to affect locomotor activity as well as circadian oscillations at tissue levels[36]. However, in this mouse model, even though the mice are behaviorally arrhythmic under constant darkness, SCN tissue explants are rhythmic with the same period length as controls. Taking into consideration that miR183/96/182 cluster was inactivated throughout the whole body, it is therefore highly unlikely that they are driving the behavioral alterations observed in our *Dicer* deficient models. Nevertheless, several miRNAs, such as miR-219[37], miR-132[37], and miR-17[38], have recently been reported to be expressed rhythmically in the SCN. miR-7a, whose predicted targets include *GABA B receptor 1*, and *Cry2*, is reported to be enriched in the SCN[39]. It might be that a combination of several SCN-specific miRNAs regulates the master clock's activities. miRNAs and transcriptomic profiling upon miRNA depletion in the SCN will help to answer the open questions.

References

1. Moore, R. Y. Organization of the mammalian circadian system. *Ciba Found. Symp.* **183**, 86–88 (1995).
2. Abrahamson, E. E. & Moore, R. Y. Suprachiasmatic nucleus in the mouse: Retinal innervation, intrinsic organization and efferent projections. *Brain Res.* **916**, 172–191 (2001).
3. Weaver, D. R. The suprachiasmatic nucleus: a 25-year retrospective. *J. Biol. Rhythms* **13**, 100–112 (1998).
4. Patton, A. P. & Hastings, M. H. The Mammalian Circadian Time-Keeping System. *J. Huntingtons. Dis.* **12**, 91–104 (2023).
5. Partch, C. L., Green, C. B. & Takahashi, J. S. Molecular architecture of the mammalian circadian clock. *Trends Cell Biol.* **24**, 90–99 (2014).

6. Zhang, R., Lahens, N. F., Ballance, H. I., Hughes, M. E. & Hogenesch, J. B. A circadian gene expression atlas in mammals: Implications for biology and medicine. *Proc. Natl. Acad. Sci.* 2–7 (2014) doi:10.1073/pnas.1408886111.

7. Ruben, M. D. *et al.* A database of tissue-specific rhythmically expressed human genes has potential applications in circadian medicine. *Sci. Transl. Med.* **10**, 1–8 (2018).

8. Mure, L. S. *et al.* Diurnal transcriptome atlas of a primate across major neural and peripheral tissues. *Science (80-.).* **359**, (2018).

9. Crosby, P. & Partch, C. L. New insights into non-transcriptional regulation of mammalian core clock proteins. *J. Cell Sci.* **133**, (2020).

10. Anna, G. & Kannan, N. N. Post-transcriptional modulators and mediators of the circadian clock. *Chronobiol. Int.* **38**, 1244–1261 (2021).

11. Lück, S., Thurley, K., Thaben, P. F. & Westermark, P. O. Rhythmic Degradation Explains and Unifies Circadian Transcriptome and Proteome Data. *Cell Rep.* 741–751 (2014) doi:10.1016/j.celrep.2014.09.021.

12. Krol, J., Loedige, I. & Filipowicz, W. The widespread regulation of microRNA biogenesis, function and decay. *Nat. Rev. Genet.* **11**, 597–610 (2010).

13. Helwak, A., Kudla, G., Dudnakova, T. & Tollervey, D. Mapping the human miRNA interactome by CLASH reveals frequent noncanonical binding. *Cell* **153**, 654–65 (2013).

14. Liu, W. & Wang, X. Prediction of functional microRNA targets by integrative modeling of microRNA binding and target expression data. *Genome Biol.* **20**, 18 (2019).

15. Park, I. *et al.* microRNA-25 as a novel modulator of circadian Period2 gene oscillation. *Exp. Mol. Med.* **52**, 1614–1626 (2020).

16. Xu, S., Witmer, P. D., Lumayag, S., Kovacs, B. & Valle, D. MicroRNA (miRNA) transcriptome of mouse retina and identification of a sensory organ-specific miRNA cluster. *J. Biol. Chem.* **282**, 25053–66 (2007).

17. Alvarez-Saavedra, M. *et al.* miRNA-132 orchestrates chromatin remodeling and translational control of the circadian clock. *Hum. Mol. Genet.* **20**, 731–51 (2011).

18. Mehta, N. & Cheng, H. Y. M. Micro-managing the circadian clock: The role of microRNAs in biological timekeeping. *J. Mol. Biol.* **425**, 3609–3624 (2013).

19. Du, N.-H., Arpat, A. B., De Matos, M. & Gatfield, D. MicroRNAs shape circadian hepatic gene expression on a transcriptome-wide scale. *Elife* **3**, e02510 (2014).

20. Husse, J., Zhou, X., Shostak, A., Oster, H. & Eichele, G. Synaptotagmin10-Cre, a driver to disrupt clock genes in the SCN. *J. Biol. Rhythms* **26**, 379–89 (2011).

21. Yoo, S.-H. *et al.* PERIOD2::LUCIFERASE real-time reporting of circadian dynamics reveals persistent circadian oscillations in mouse peripheral tissues.

Proc. Natl. Acad. Sci. U. S. A. **101**, 5339–46 (2004).

22. Malyutina, A., Tang, J. & Pessia, A. drda: An R Package for Dose-Response Data Analysis Using Logistic Functions. *J. Stat. Softw.* **106**, 1–26 (2023).

23. Ohta, H., Yamazaki, S. & McMahon, D. G. Constant light desynchronizes mammalian clock neurons. *Nat. Neurosci.* **8**, 267–269 (2005).

24. Oishi, K., Higo-Yamamoto, S., Yamamoto, S. & Yasumoto, Y. Disrupted light–dark cycle abolishes circadian expression of peripheral clock genes without inducing behavioral arrhythmicity in mice. *Biochem. Biophys. Res. Commun.* **458**, 256–261 (2015).

25. Roper, L. K., Briguglio, J. S., Evans, C. S., Jackson, M. B. & Chapman, E. R. Sex-specific regulation of follicle-stimulating hormone secretion by synaptotagmin 9. *Nat. Commun.* **6**, 8645 (2015).

26. Ono, D., Honma, K.-I. & Honma, S. Roles of Neuropeptides, VIP and AVP, in the Mammalian Central Circadian Clock. *Front. Neurosci.* **15**, 650154 (2021).

27. Bernstein, E. *et al.* Dicer is essential for mouse development. *Nat. Genet.* **35**, 215–7 (2003).

28. Chen, R., D'Alessandro, M. & Lee, C. miRNAs Are Required for Generating a Time Delay Critical for the Circadian Oscillator. *Curr. Biol.* 1–10 (2013) doi:10.1016/j.cub.2013.08.005.

29. Davis, T. H. *et al.* Conditional loss of Dicer disrupts cellular and tissue morphogenesis in the cortex and hippocampus. *J. Neurosci.* **28**, 4322–30 (2008).

30. Pilorz, V., Kolms, B. & Oster, H. Rapid Jetlag Resetting of Behavioral, Physiological, and Molecular Rhythms in Proestrous Female Mice. *J. Biol. Rhythms* **35**, 612–627 (2020).

31. Jais, A. *et al.* PNOCARC Neurons Promote Hyperphagia and Obesity upon High-Fat-Diet Feeding. *Neuron* **106**, 1009-1025.e10 (2020).

32. Wang, C. *et al.* TAp63 contributes to sexual dimorphism in POMC neuron functions and energy homeostasis. *Nat. Commun.* **9**, 1544 (2018).

33. Yamaguchi, Y. *et al.* Mice genetically deficient in vasopressin V1a and V1b receptors are resistant to jet lag. *Science (80-.).* **342**, 85–90 (2013).

34. Hatori, M. *et al.* Lhx1 maintains synchrony among circadian oscillator neurons of the SCN. *Elife* **3**, e03357 (2014).

35. Soula, A. *et al.* Small RNA-Seq reveals novel miRNAs shaping the transcriptomic identity of rat brain structures. *Life Sci. alliance* **1**, e201800018 (2018).

36. Zhou, L. *et al.* A genome-wide microRNA screen identifies the microRNA-183/96/182 cluster as a modulator of circadian rhythms. *Proc. Natl. Acad. Sci. U. S. A.* **118**, 1–9 (2021).

37. Cheng, H.-Y. M. *et al.* microRNA modulation of circadian-clock period and entrainment. *Neuron* **54**, 813–29 (2007).

38. Gao, Q., Zhou, L., Yang, S.-Y. & Cao, J.-M. A novel role of microRNA 17-5p in the modulation of circadian rhythm. *Sci. Rep.* **6**, 30070 (2016).

39. Herzer, S., Silahtaroglu, A. & Meister, B. Locked Nucleic Acid-Based In Situ Hybridisation Reveals miR-7a as a Hypothalamus-Enriched MicroRNA with a Distinct Expression Pattern. *J. Neuroendocrinol.* **24**, 1492–1504 (2012).

Figure legends

Figure 1: SCN-specific *Dicer* KO had shorter period length. (A) Summary of free-running period length under constant darkness (DD) measured by wheel running activities. (B) Examples of two KO mice. (C) Examples of two control mice.

Figure 2: SCN-specific Dicer KO reentrained faster to jetlag. (A) Onset of locomotor activities upon 6h-advanced jetlag at day 6 (control n = 10, KO n = 5, data is mean ± sem). (B) Onset of locomotor activities upon 6h-delayed jetlag at day 6 (control n = 5, KO n = 3, data is mean ± sem). (C) Examples of advanced jetlag for KO mice. (D) Examples of advanced jetlag for control mice.

Figure 3: KO mice had larger onset variation than controls. (A) Standard deviation of onset time in minutes (measured from wheel running activities under LD = 12:12, KO n = 5, ctrl n = 10, data = mean ± sd). (B) Absolute difference to light off time in minutes (measured from wheel running activities under LD = 12:12, KO n = 5, ctrl n = 10, data = mean ± sd). (C) Standard deviation of onset time in minutes (measured from infrared detector under LD = 12:12, KO n = 4, ctrl n = 9, data = mean ± sd). (D) Standard deviation of onset time in hours (measured from wheel running activities under LD = 11:11, KO n = 4, ctrl n = 10, data = mean ± sd).

Figure 4: KO mice adapted worse to different day length. (A) Examples of wheel running activities from KO mice. (B) Examples of wheel running activities from control mice.

Figure 5: KO mice had arrhythmic/ultradian rhythms in LL with no light masking. (A) Examples of wheel running activities from KO mice. (B) Examples of wheel running activities from control mice.

Figure 6: KO mice were masked by light to some extent under LD = 3:3 condition, showing that the animals were not irresponsive to light. Animals were kept under DD for 20 days before light conditions were changed as indicated in the figures. Examples of wheel running activities from KO mice (A) and control (B).

Figure 7: SCN from KO mice also had shorter period length. (A) period length of *ex vivo* culture of tissue slices from different tissues. (B) Examples of rhythms from SCN and lung. SCN rhythms from KO mice were more difficult to obtain than those from controls. Tissue explants from the same animals share the same colors.

Figure 8: When KO is induced by injection of $Dicer^{flox}$ mice with AVV expressing *hSyn-Cre*, KO mice had variable phenotypes, but eventually got arrhythmic. (A) Control injection. (B) *hSyn-Cre* injection. Yellow part denotes when light was on.

Figure 9: Suggestive evidence of SCN firing being less synchronized in KO mice than in control (n=1 each). SCN slides on MEA, annotation of electrodes that overlapped with SCN region (purple circles), and SCN firing frequencies across time points for KO (A) and control (B). Electrodes (6x10) are annotated as following: SCN TRUE if the SCN is located above that electrode, SCN FASLE if not; MEA TRUE if the electrode is technically functional, MEA FALSE if not. For the time series plots, only electrodes that were located below the SCN and technically functional were color-coded based on the firing frequencies.

Figure S1: Confirmation of recombination by PCR analysis. (A) Schematic of genomic locus. Primers *Dicer*F1 and *Dicer*Del produce a fragment of 601 nt length. (B) Gel picture of the recombined *Dicer* fragment detected in the olfactory bulb of the knockout (KO) animal but not in the ear.

Figure S2: Examples of onset detection in KO and control mice. Activities were recorded using infrared detectors.

Figure S3: Example of VIP expression reduction in KO mice (ZT7, n=1). One should note that the optical chiasm in the knockout SCN was not present in the slide, indicating that one part of the SCN might have been ripped off.

Figure S4: Gender differences in phenotypes of knockout animals. (A) Female KO were extremely overweighted. Left: control, right: KO female. (B) Period length of tissue explants from control and KO females. Tissue explants from the same animals share the same colors.

Figure 1

A

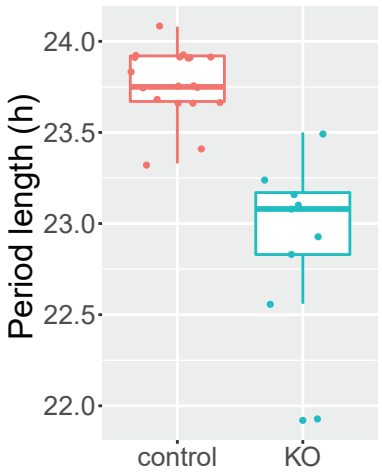

B

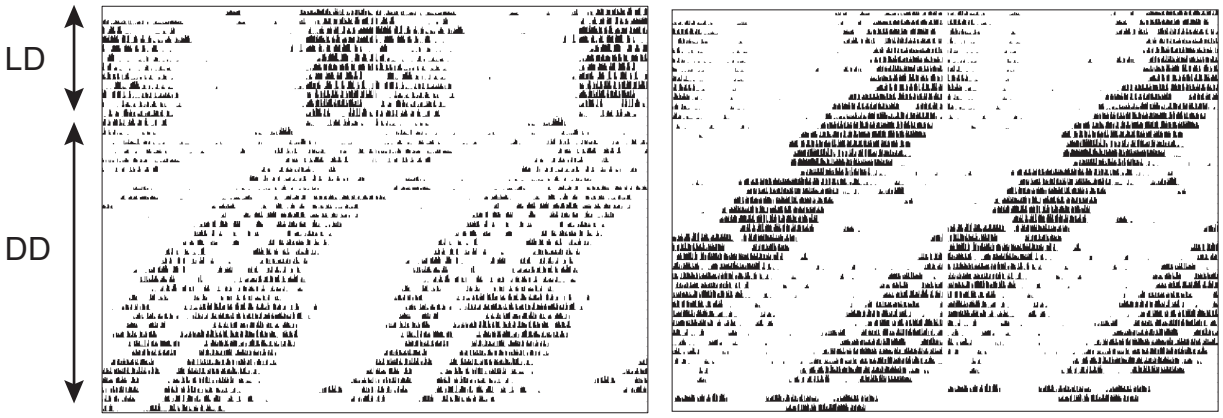

C

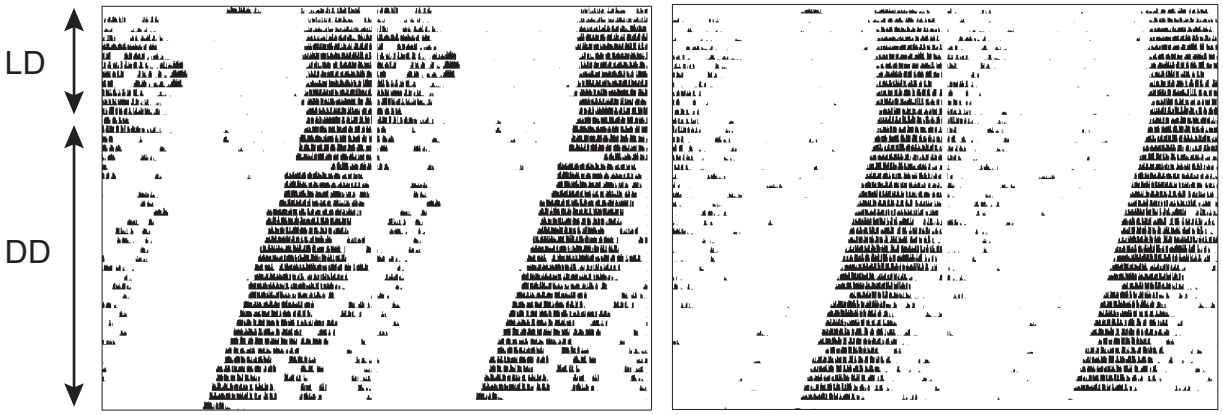

Figure 2

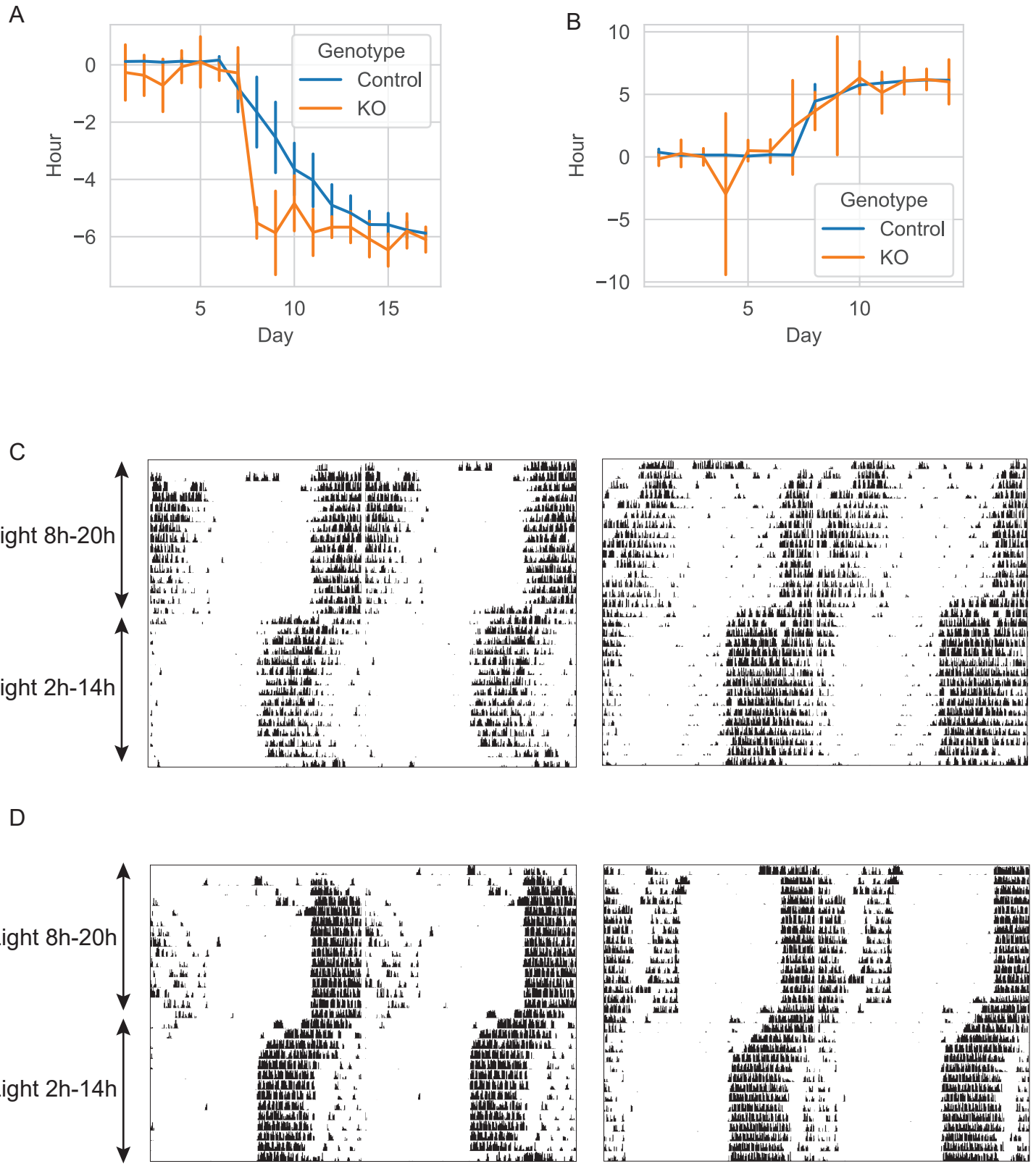
A
Genotype
Control
KO
Hour
0
−2
−4
−6
5
10
15
Day
B
Genotype
Control
KO
Hour
10
5
0
−5
−10
5
10
Day
C
Light 8h-20h
Light 2h-14h
D
Light 8h-20h
Light 2h-14h

Figure 3

A

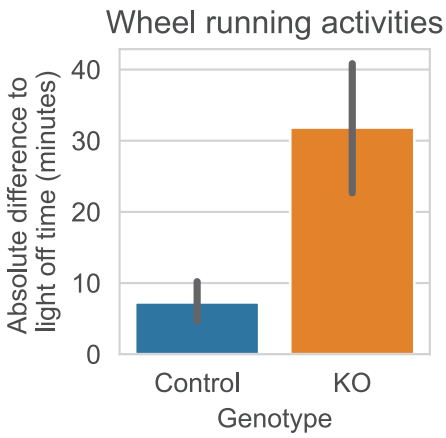

B

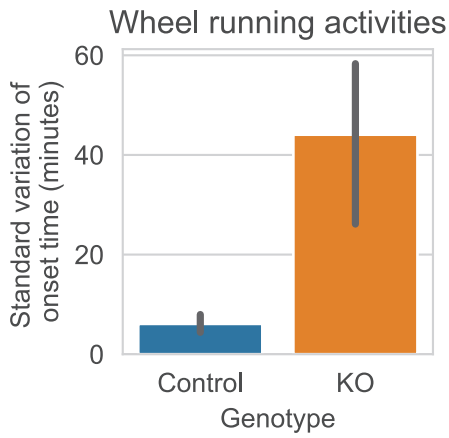

C

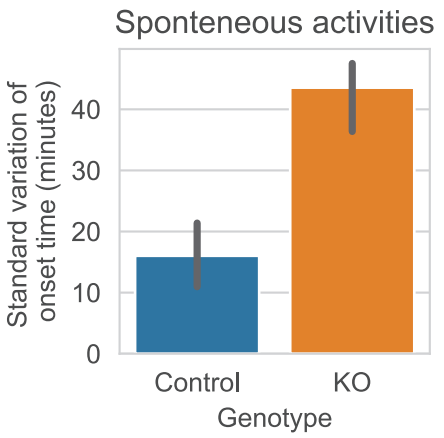

D

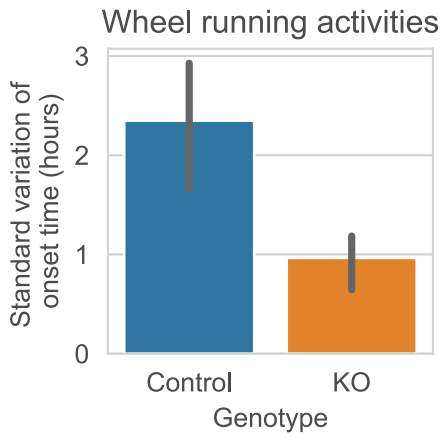

Figure 4

A

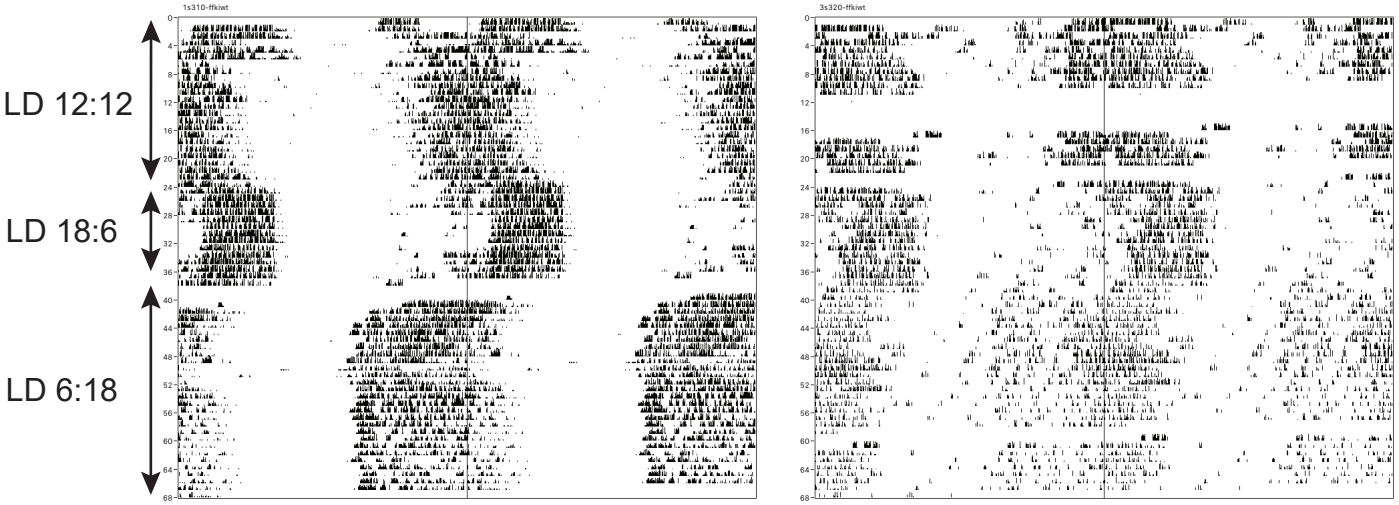
LD 12:12
LD 18:6
LD 6:18
1s310-ffkiwt
3s320-ffkiwt

B

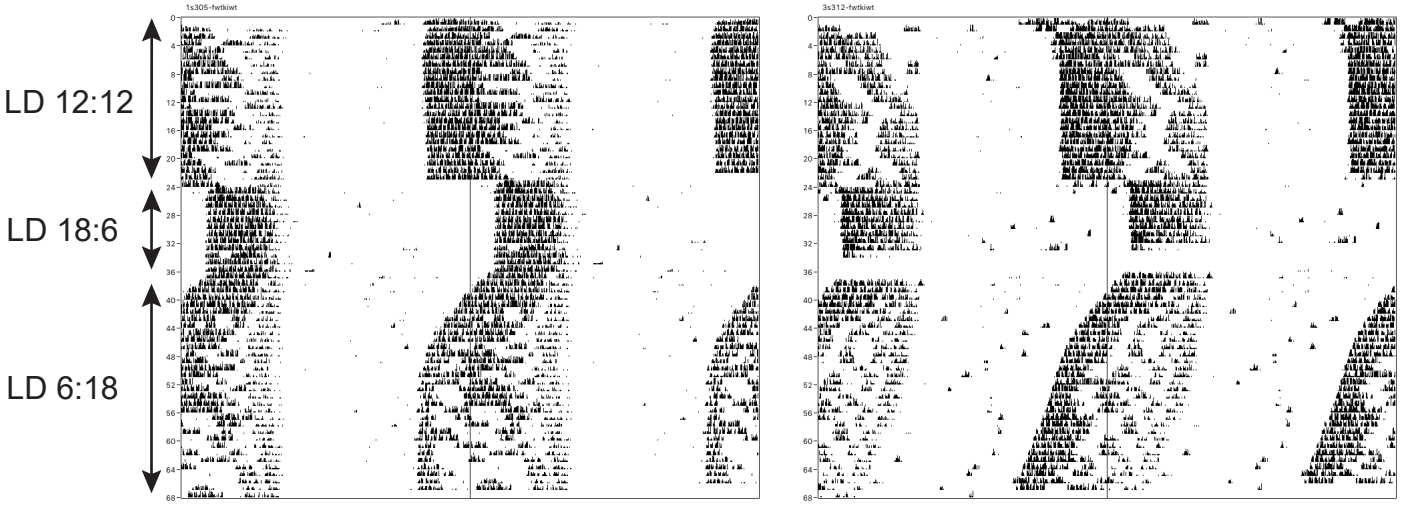
LD 12:12
LD 18:6
LD 6:18
1s305-fwtkiwt
3s312-fwtkiwt

Figure 5

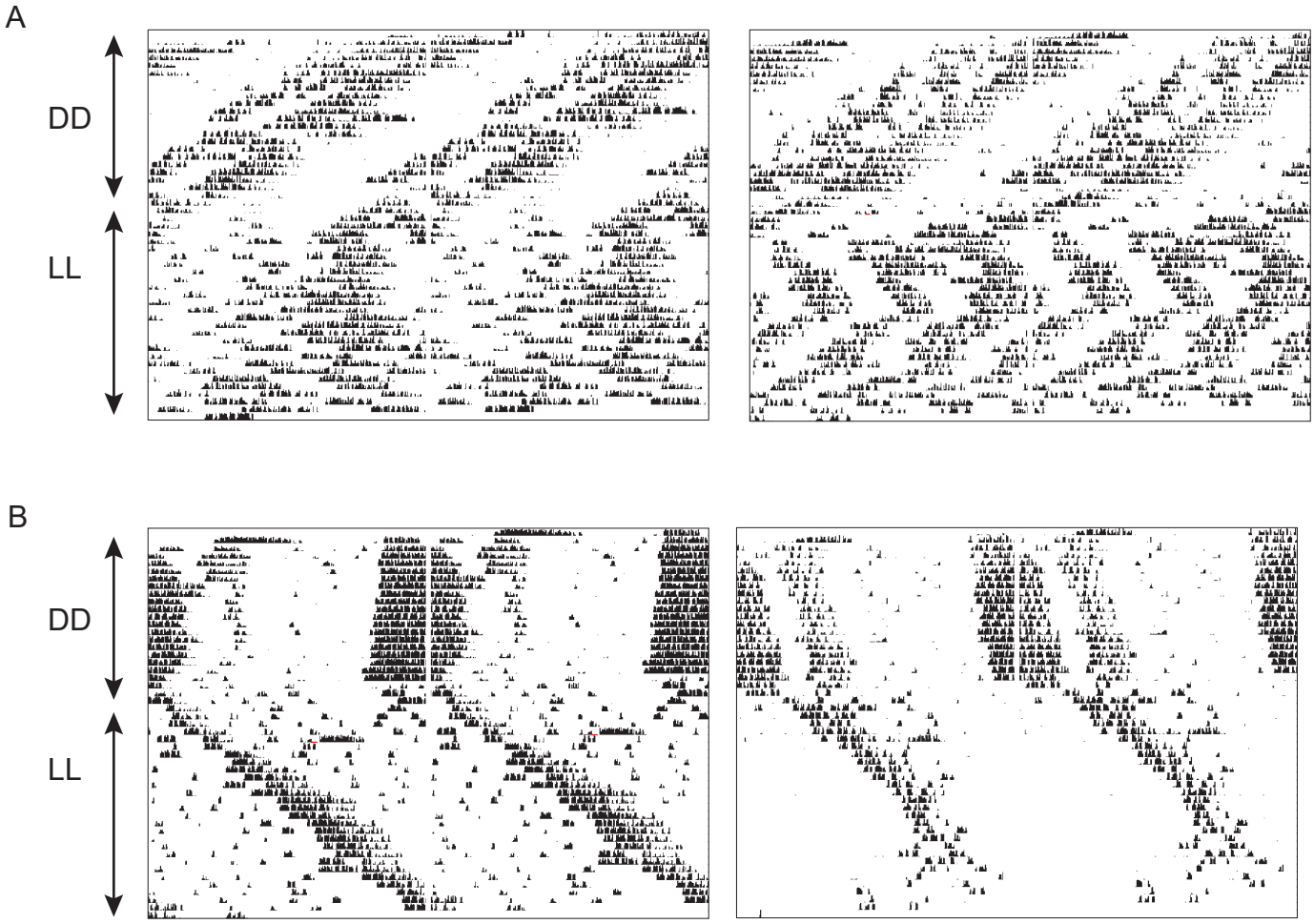

Figure 6

A

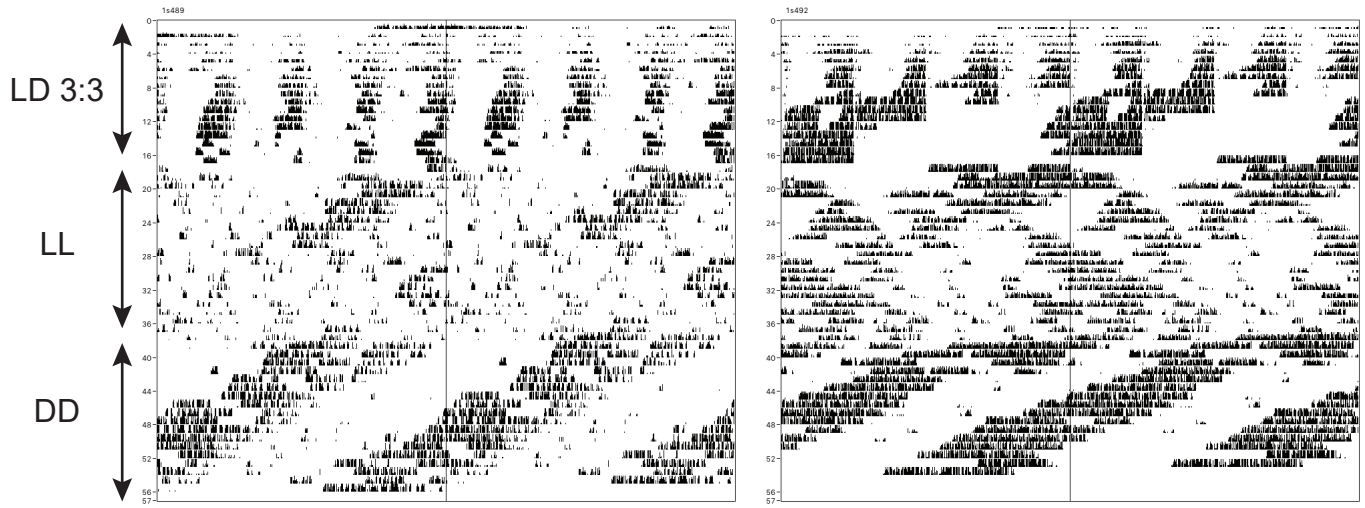

B

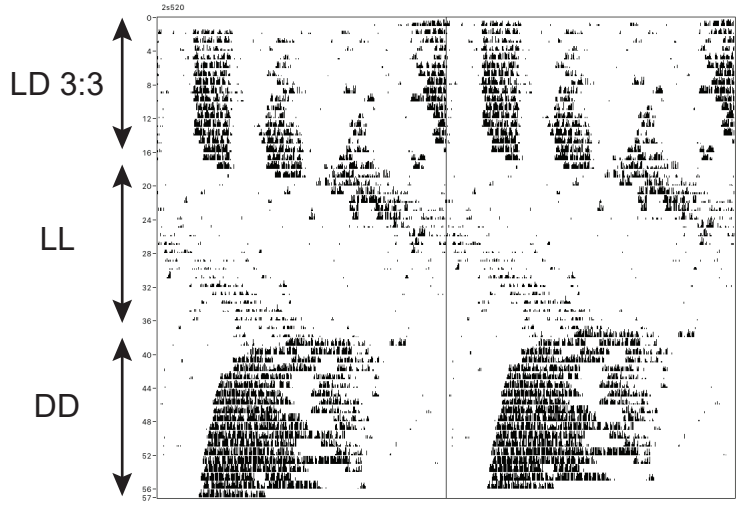

Figure 7

A

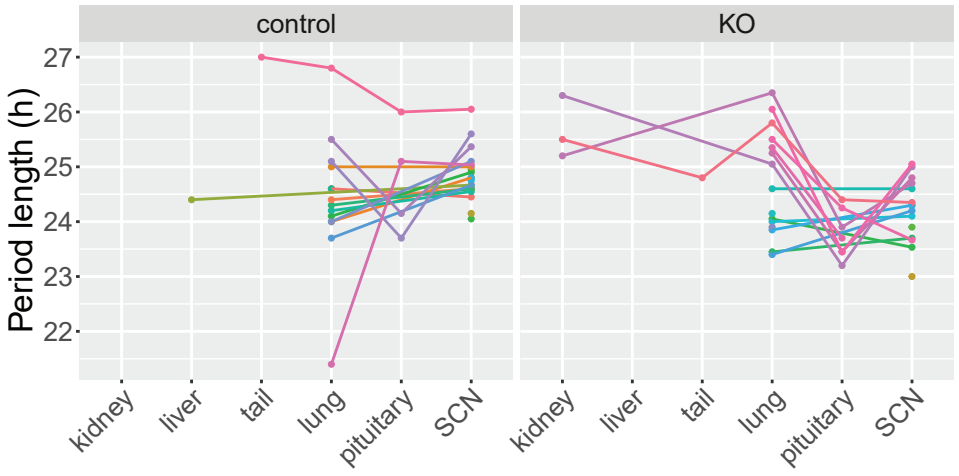
control
KO
Period length (h)
27
26
25
24
23
22
kidney
liver
tail
lung
pituitary
SCN

B

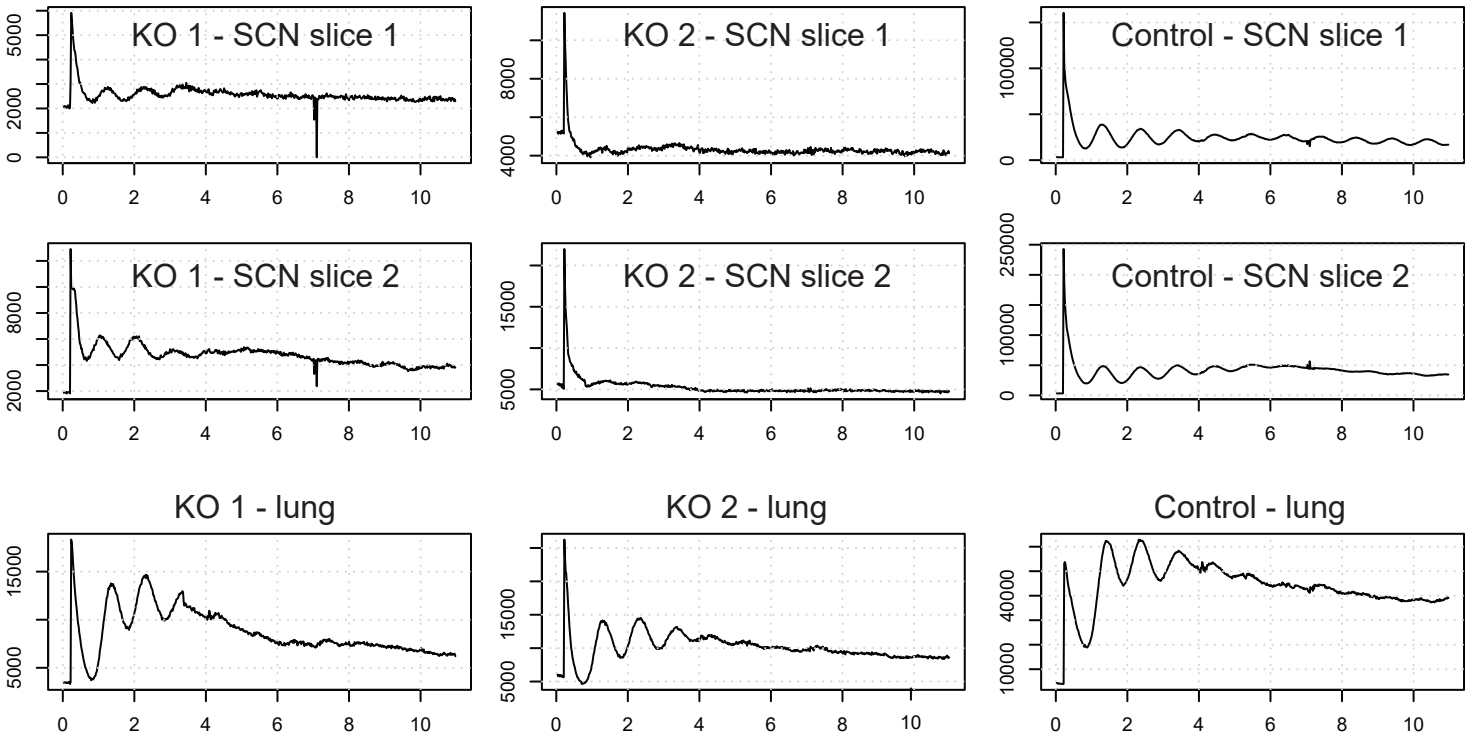
KO 1 - SCN slice 1
KO 2 - SCN slice 1
Control - SCN slice 1
KO 1 - SCN slice 2
KO 2 - SCN slice 2
Control - SCN slice 2
KO 1 - lung
KO 2 - lung
Control - lung

Figure 8

A

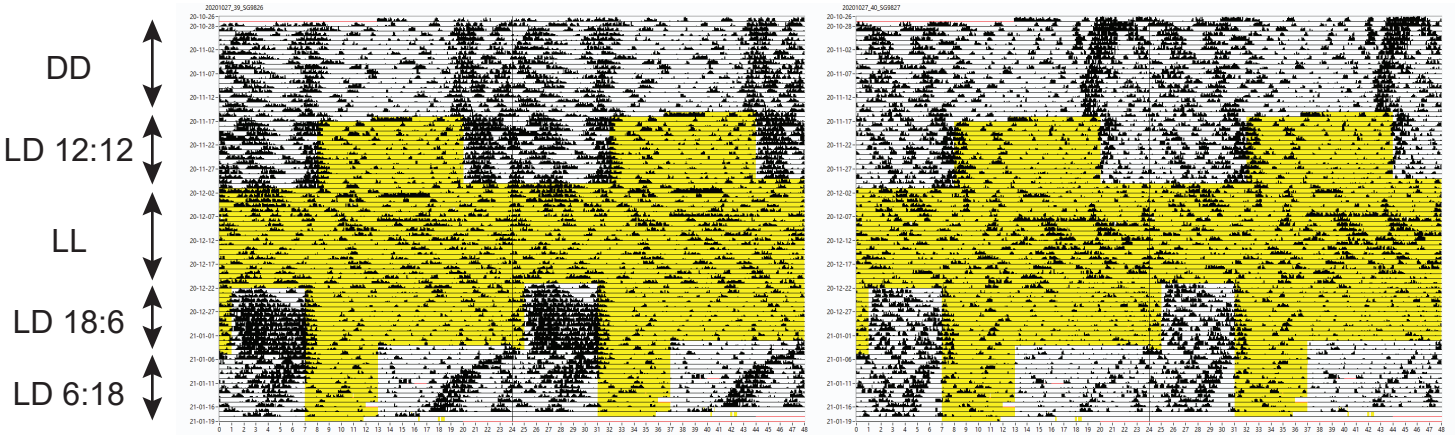

B

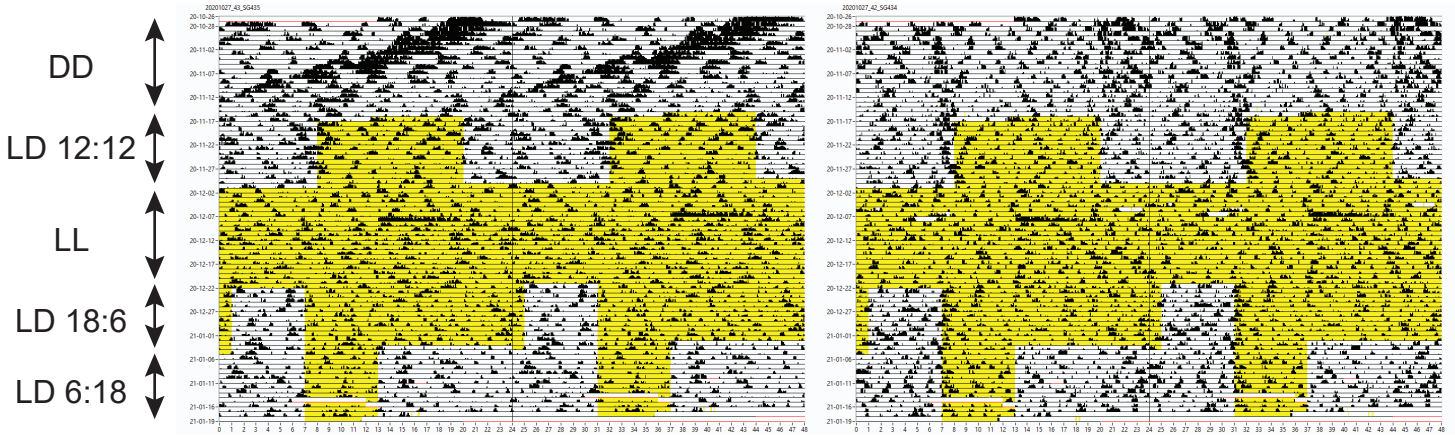

Figure 9

A

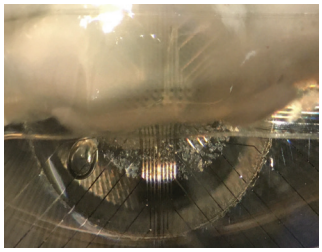

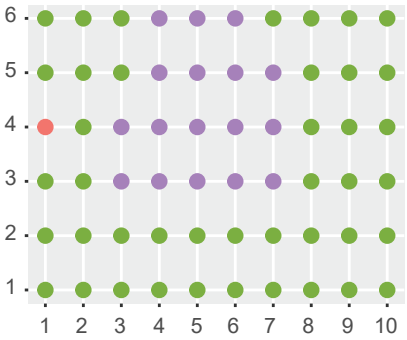

Electrode
- SCN:FALSE; MEA:FALSE
- SCN:FALSE; MEA:TRUE
- SCN:TRUE; MEA:FALSE
- SCN:TRUE; MEA:TRUE

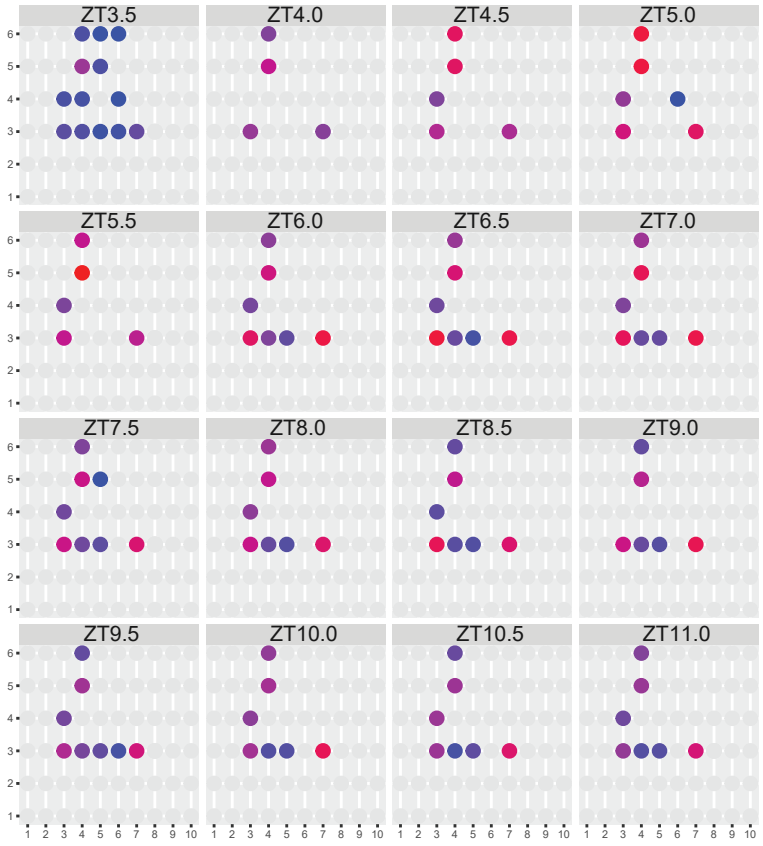

B

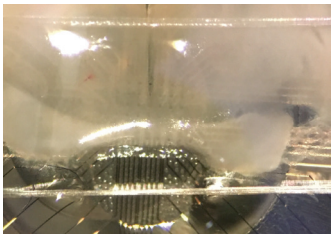

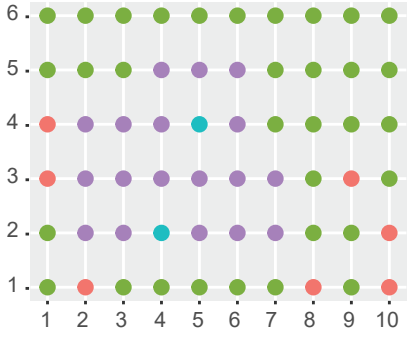

Electrode
- SCN:FALSE; MEA:FALSE
- SCN:FALSE; MEA:TRUE
- SCN:TRUE; MEA:FALSE
- SCN:TRUE; MEA:TRUE

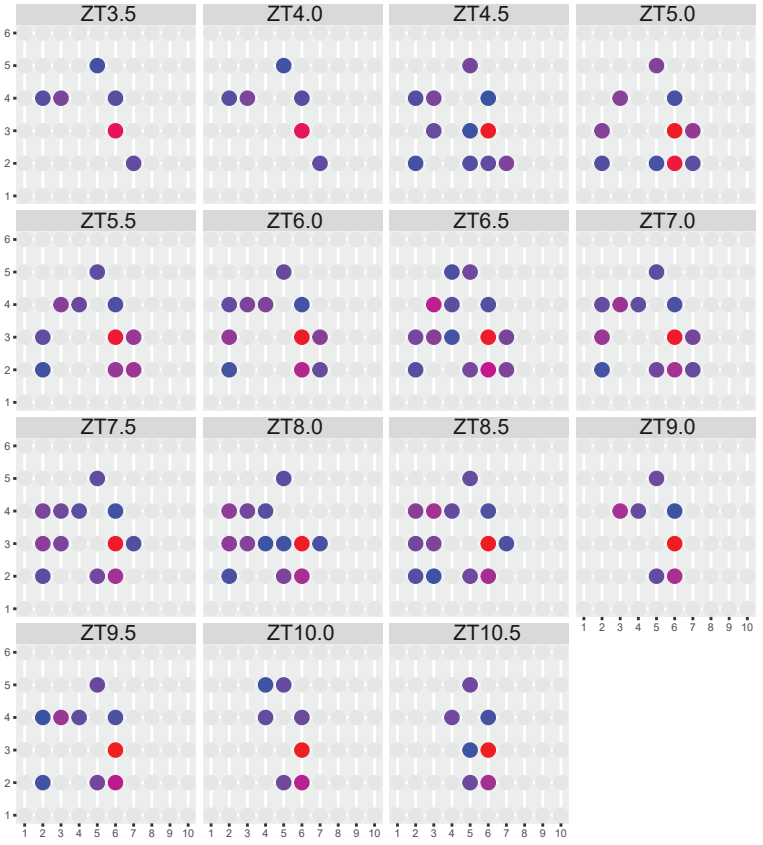

Figure S1

A

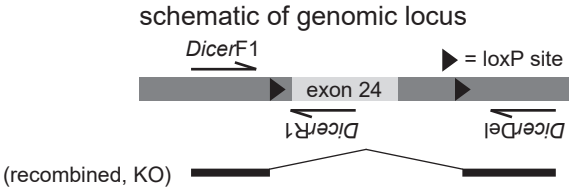
schematic of genomic locus
DicerF1
= loxP site
exon 24
DicerR1
DicerDel
(recombined, KO)

B

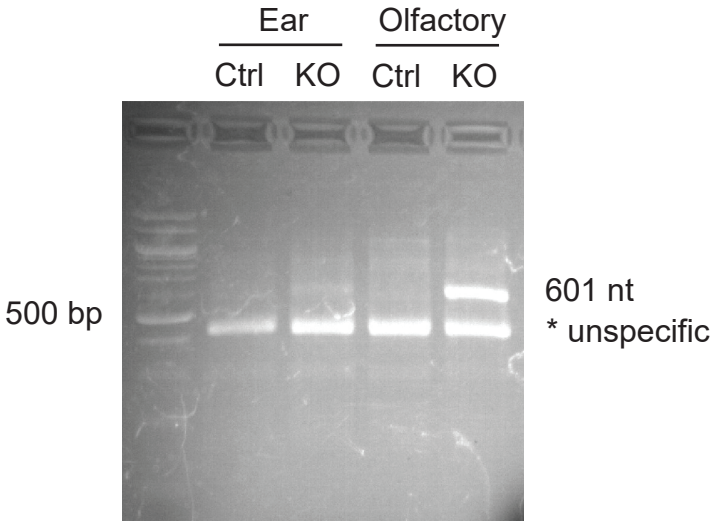
Ear
Olfactory
Ctrl
KO
Ctrl
KO
500 bp
601 nt
* unspecific

Figure S2

A

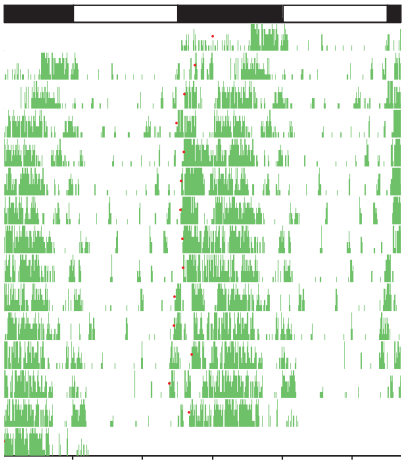

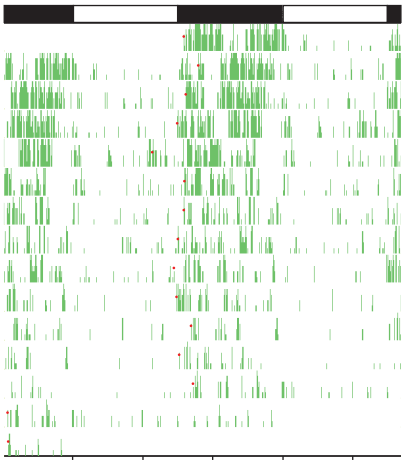

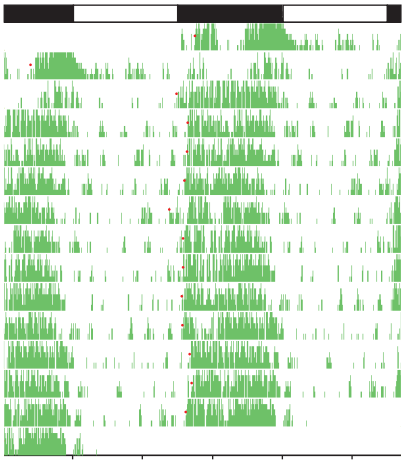

B

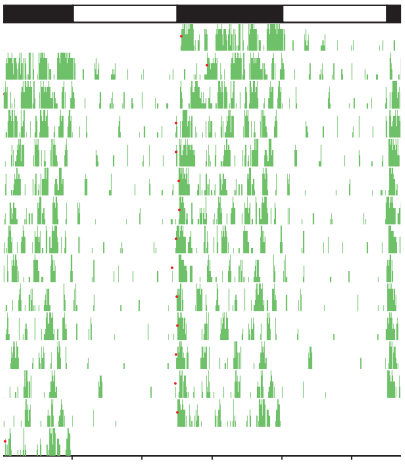

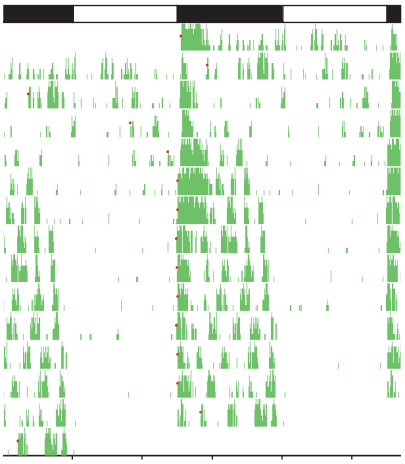

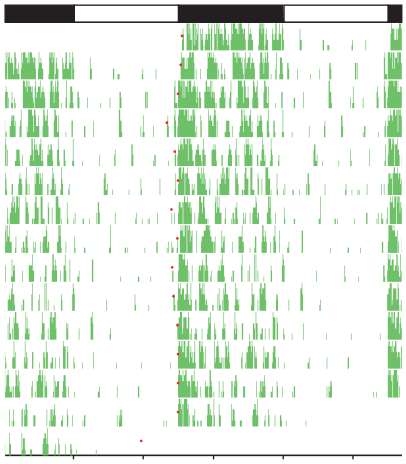

Figure S3

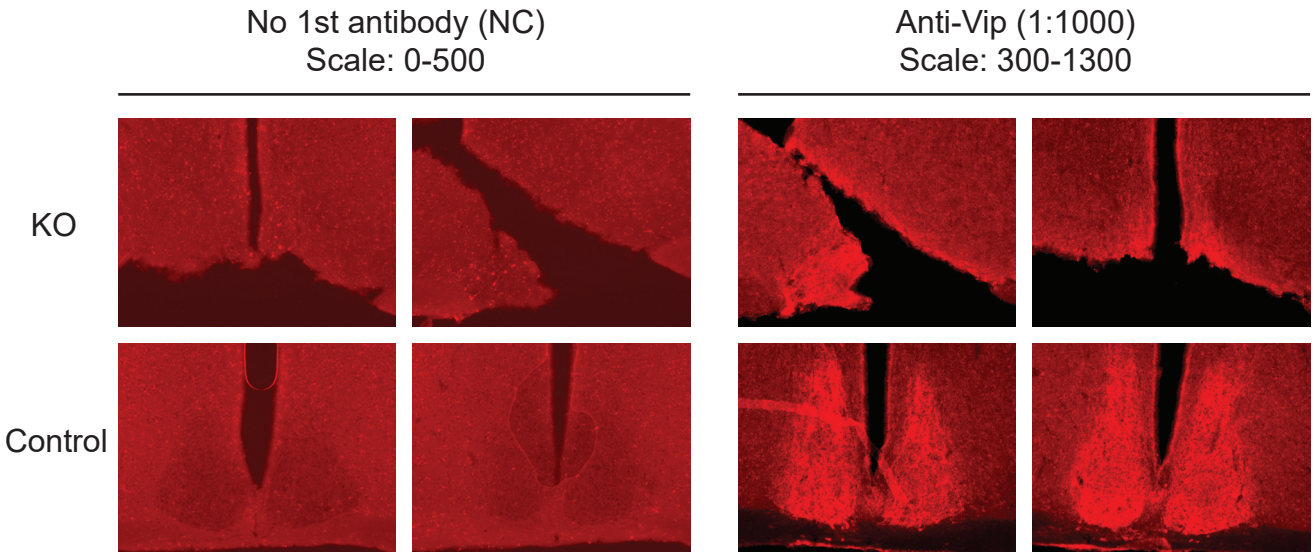
No 1st antibody (NC)
Scale: 0-500
Anti-Vip (1:1000)
Scale: 300-1300
KO
Control

Figure S4

A

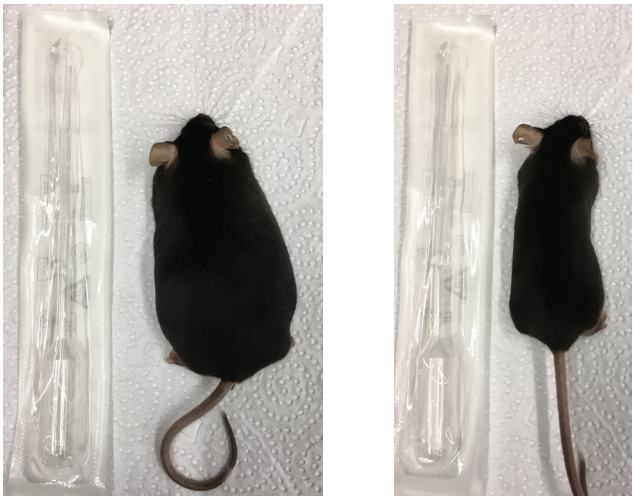

B

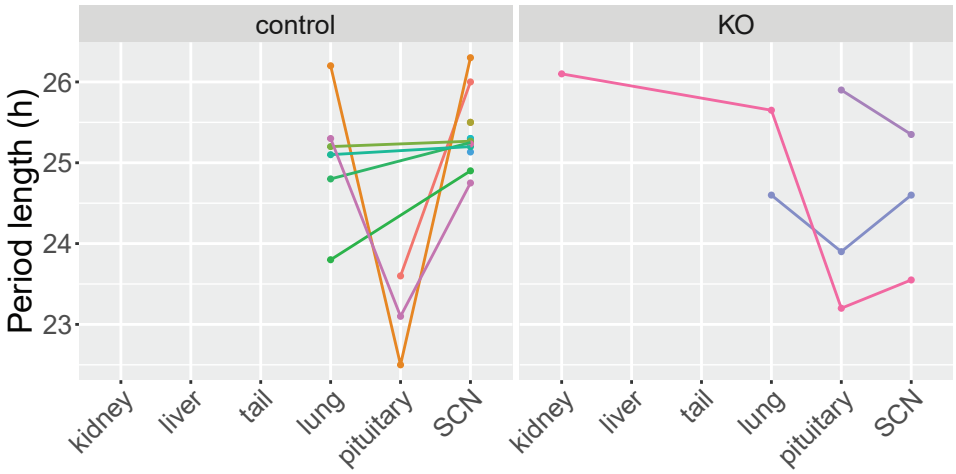
control
KO
Period length (h)
26
25
24
23
kidney
liver
tail
lung
pituitary
SCN